Available online at www.sciencedirect.com
ScienceDirect
Journal of Molecular Structure 873 (2008) 17–28
Journal of MOLECULAR STRUCTURE
www.elsevier.com/locate/molstruc

Synthesis, characterization and molecular sensing behavior of [$ZnCl_2(\eta^3$-N,N,O-dpkbh)] (dpkbh = di-2-pyridyl ketone benzoyl hydrazone)

Mohammed Bakir *, Orville Green, Willem H. Mulder

Department of Chemistry, The University of the West Indies – Mona Campus, Kingston 7, Jamaica

Received 13 January 2007; accepted 1 March 2007
Available online 12 March 2007

Abstract

The reaction between $ZnCl_2$ and di-2-pyridyl ketone benzoyl hydrazone (dpkbh) in acetonitrile under ultrasonic or reflux conditions gave [$ZnCl_2(\eta^3$-N,N,O-dpkbh)] in good yield. The identity of the compound was established from the results of its elemental analysis and a number of spectroscopic measurements. Solid-state infrared spectra of [$ZnCl_2(\eta^3$-N,N,O-dpkbh)] reveal the coordination of dpkbh, the presence of the amide proton and binding of the oxygen atom of dpkbh. ^{1}H NMR spectra of [$ZnCl_2(\eta^3$-N,N,O-dpkbh)] show sensitivity to solvent and temperature variations and confirm the coordination of dpkbh. The electronic absorption spectra of [$ZnCl_2(\eta^3$-N,N,O-dpkbh)] in non-aqueous media show high sensitivity to changes in their surroundings and divulge two interlocked intra-ligand-charge transfer (ILCT) transitions of the donor–acceptor type between 300 and 500 nm. Optical measurements show reversible inter-conversion between two forms of [$ZnCl_2(\eta^3$-N,N,O-dpkbh)] that may be due to complex–substrate interactions and thermodynamic analysis gave changes in enthalpy (ΔH^θ) of −23.3 and +14.1 kJ mol^{-1}, entropy (ΔS^θ) of −51 and +31 J mol^{-1}K^{-1}, and free energy (ΔG^θ) of −8.16 and +4.54 kJ mol^{-1} at 298.15 K in DMF and DMSO, respectively. Substrates in concentrations as low as 10^{-5} M can be detected and determined using [$ZnCl_2(\eta^3$-N,N,O-dpkbh)] in polar solvents. A provisional model for the binding of substrate to [$ZnCl_2(\eta^3$-N,N,O-dpkbh)] is developed and a binding constant in the range 6000–8000 M^{-1} is obtained in the case of $ZnCl_2$ in DMSO. Electrochemical measurements on [$ZnCl_2(\eta^3$-N,N,O-dpkbh)] in DMF show irreversible metal and ligand-based redox processes, and electrochemical reactions of dpkbh with $ZnCl_2$ show facile coordination of $ZnCl_2$ and formation of [$ZnCl_2(\eta^3$-N,N,O-dpkbh)]. X-ray structural analysis done on a crystal grown from a DMF solution of [$ZnCl_2(\eta^3$-N,N,O-dpkbh)] confirmed the identity of [$ZnCl_2(\eta^3$-N,N,O-dpkbh)] and shows an extensive network of non-covalent interactions that connects all molecules.

Keywords: Hydrazone metal complexes; Di-2-pyridyl ketone benzoyl hydrazone; Sensors; Synthesis and crystal structure

1. Introduction

Di-2-pyridyl ketone [$(C_5H_4N)_2C{=}O$] and its oxime, and hydrazone derivatives (see Scheme 1) and their metal compounds continue to attract much attention because of their reactivity patterns, physical properties and relevance in many important chemical and biological processes [1–7]. We have been interested in the chemistry of di-2-pyridyl ketone (dpk) derivatives (see Scheme 1) and described the synthesis and characterization of a series of compounds of di-2-pyridyl ketone derivatives [8–27]. Spectroscopic measurements on di-2-pyridyl ketone hydrazones revealed their sensitivity to changes in their surroundings and X-ray structural analysis uncovered a web of non-covalent interactions, which may account for this sensitivity. The ligand di-2-pyridyl ketone benzoyl hydrazone (dpkbh) is widely used as a sensitive analytical reagent for the determination of trace amounts of metal ions in solutions [28,29]. Bidentate N,N and tridentate N,N,O coordination

* Corresponding author. Tel.: +1 876 935 8164; fax: +1 876 977 1835.
E-mail address: mohammed.bakir@uwimona.edu.jm (M. Bakir).

0022-2860/$ - see front matter © 2007 Elsevier B.V. All rights reserved.
doi:10.1016/j.molstruc.2007.03.001

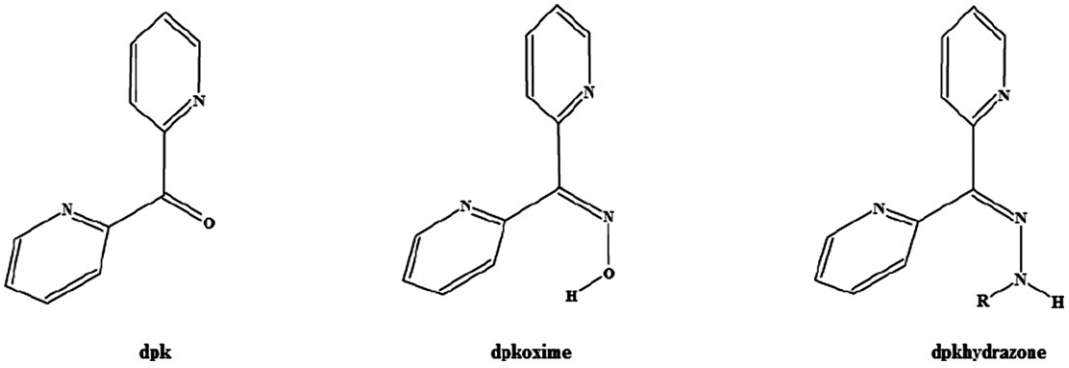

Scheme 1. Di-2-pyridyl ketone and its oxime, hydrazone derivatives.

modes were reported for dpkbh [11,12,30–32]. In recent reports, rhenium-tricarbonyl compounds of the type *fac*-[$Re(CO)_3(\eta^2$-N,N-dpkbh)X] where X = Cl or Br were reported with dpkbh binding to the rhenium atom through the nitrogen atoms of the pyridine rings or through one nitrogen atom of a pyridine ring and the nitrogen atom of the hydrazone backbone as shown in Scheme 2 [11,12,30]. The synthesis and cytotoxicity of a series of metal compounds of the tridentate N,N,O dpkbh anion of the type $[M(\eta^3$-N,N,O-dpkbh$)_2]^n$ where M is a first-row transition element along with their potential as lipophilic transport shuttles that allow entrance to the cell and enable the delivery of both the ligand and metal to inhibit proliferation of tumor cells were reported [31,32].

Spectroscopic measurements on dpkbh and *fac*-[$Re(CO)_3$(dpkphh)Cl] in non-aqueous solvents show two interlocked charge transfer transitions that are sensitive to slight changes in their surroundings and substrates in the range 1×10^{-5}–1×10^{-9} M were detected and determined using dpkbh and its rhenium derivatives [10–12]. In an effort to elucidate the molecular sensing behavior of dpkbh and its metal compounds, herein we report on the synthesis, spectroscopic, electrochemical, and optosensing properties of a zinc compound of η^3-N,N,O-dpkbh, [$ZnCl_2(\eta^3$-N,N,O-dpkbh)].

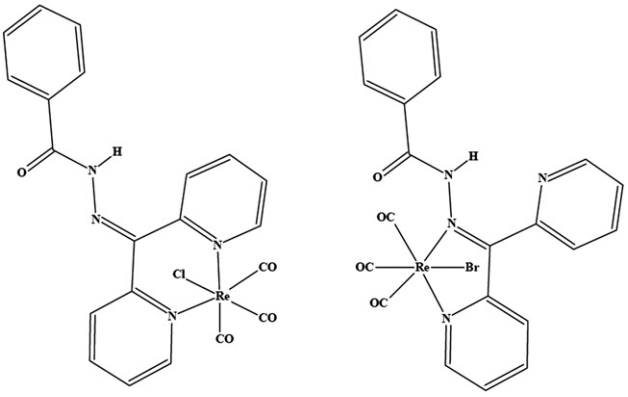

Scheme 2. Views of *fac*-[$Re(CO)_3(\eta^2$-N,N-dpkbh)X].

2. Experimental

2.1. Reagents

All reagents were obtained from commercial sources and used without further purification. The ligand dpkbh was prepared following a standard literature procedure [10].

2.1.1. Preparation of [$ZnCl_2(\eta^3$-N,N,O-dpkbh)]

A mixture of $ZnCl_2$ (100 mg, 0.73 mmol), dpkbh (150 mg, 0.81 mmol) and acetonitrile (50 mL) was allowed to stand in an ultrasonic bath or refluxed in air for 3 h. The resulting yellow precipitate was filtered off, washed with hexane, diethyl ether and dried; yield 190 mg (80%) (found: C, 49.29; H, 3.26; N, 12.79. $C_{18}H_{14}Cl_2N_4OZn$ requires C, 49.29; H, 3.22; N, 12.77%). Infrared data (KBr disk, cm^{-1}): ν(NH) 3450 (broad), ν(CH) 3057, ν(C=O) 1638, ν(py) and ν(ph) 1594 and 1575. UV–vis {λ/nm, ($\varepsilon \pm 100$/$cm^{-1}\,M^{-1}$)} in the concentration range 2×10^{-5}–2×10^{-6} M: in DMF 397 (20,000) and 324 (3485); in DMSO 397 (14,323), 324 (2880), 276 (2850); CH_3CN 393 (1680), 355 (sh) 336 (15,460), 290 (sh), 283 (sh), 270 (12,960) and 235 (sh), 225 (14,460); CH_2Cl_2 396 (315), 358(sh), 342 (18,765), 290 (sh), 282 (sh) and 273 (12,977). ^{1}H NMR (δ, ppm): in DMF-d_7 at 30 °C 14.88 (s, 1H, NH), 9.05 (d, 1H), 8.77 (d, 1H), 8.18 (t, 1H), 8.14 (t, 1H), 8.08 (d, 21H), 7.99 (d, 1H), 7.77–767 (overlapped t's and d's, 3H) and 7.65 (t, H). ^{1}H NMR (δ ppm): in DMSO-d_6 at 30 °C 15.05 (NH), 8.95 (d, 1H), 8.65 (d, 1H), 8.06 (d, t, 2H), 8.02 (d, 1H), 7.96–7.89 (d, 31H), 7.70–7.50 (overlapped t's and d's, 3H) and 7.65 (t, 8H).

2.2. X-ray crystallography

A single crystal isolated from the filtrate of the reaction mixture was selected and mounted on a glass fiber with epoxy cement. A Bruker SMART APEX CCD area detector diffractometer with a MoK_α radiation and a graphite monochromator was used for data collection and the SHELXTL software package version 5.1 was used for structure solution [33,34]. Cell parameters and other crys-

tallographic information are given in Table 1, along with additional details concerning data collection. All non-hydrogen atoms were refined with anisotropic thermal parameters. All other H-atom positions were refined assuming idealized geometry, with C–H distance of 0.93 Å and N–H distance of 0.86 Å.

2.3. Optical sensing studies

A stock solution of [$ZnCl_2$(η^3-N,N,O-dpkbh)] in a polar non-aqueous solvent, and stock solutions of a stimulus ($NaBH_4$, $NaBF_4$ or $ZnCl_2$) in a polar non-aqueous solvent were prepared separately. Optical changes (electronic absorption spectral changes) were measured on solutions prepared by mixing appropriate volumes of [$ZnCl_2$(η^3-N,N,O-dpkbh)] and stimulus solutions to prepare the desired solutions (see figure captions for details). All measurements were made at room temperature.

2.4. Equipment

Electronic absorption spectra were recorded on a HP-8452A spectrophotometer or a Perkin-Elmer UV/vis/NIR spectrometer λ-19. Baseline corrections on blank solvents were recorded prior to measurements. A Lauda–Brinkmann RM6 circular bath was used for temperature control. Solution ^{1}H NMR spectra were recorded on a Bruker ACE 500-MHz Fourier-transform spectrometer and referenced to the residual protons in the incompletely deuteriated solvent. Infrared spectra were recorded as KBr pellets on a Perkin-Elmer Spectrum 1000 FT-IR Spectrometer. Electrochemical measurements were performed with the use of a Princeton Applied Research (PAR) Model 173 potentiostat/galvanostat and Model 276 interface in conjunction with a 286 PC. Data were acquired with the EG&G PARC Headstart program and manipulated using the Microsoft Excel Program. Measurements were performed in solutions that were 0.1 M in [N(n-Bu)$_4$][PF_6]. The $E_{p,a}$, $E_{p,c}$ and $E_p = (E_{p,a} + E_{p,c})/2$ values were referenced to the quasi-reversible silver electrode at room temperature and are uncorrected for junction potentials.

2.5. Molecular orbitals calculations

PM3 semi-empirical molecular orbital calculations using default parameters on the lowest electronic state with configurational interaction of $1 \rightarrow 1$ in the singly excited state were conducted on a Hyperchem molecular modeling program. A Polak–Ribiere energy minimized model using AMBER force field was used.

3. Results and discussion

When di-2-pyridyl ketone benzoyl hydrazone was allowed to react with $ZnCl_2$ in acetonitrile under reflux or ultrasonic radiation [$ZnCl_2$(η^3-N,N,O-dpkbh)] was isolated in good yield. The formulation of the compound as [$ZnCl_2$(η^3-N,N,O-dpkbh)] was based upon the results of its elemental analysis, a number of spectroscopic measurements, and X-ray structural analysis done on a crystal grown from a DMF solution of [$ZnCl_2$(η^3-N,N,O-dpkbh)] when allowed to stand at room temperature for several

Table 1
Crystal data and structure refinement for [$ZnCl_2$(η^3-N,N,O-dpkbh)]

Empirical formula	$C_{18}H_{14}Cl_2N_4OZn$
Formula weight	438.60
Temperature	273(2) K
Wavelength	0.71073 Å
Crystal system, space group	Monoclinic, $P2_1/n$
Unit cell dimensions	$a = 8.341(2)$ Å, $\alpha = 90°$
	$b = 13.911(4)$ Å, $\beta = 93.864(5)°$
	$c = 15.968(4)$ Å, $\gamma = 90°$
Volume	1848.7(9) Å^3
Z, calculated density	4, 1.576 mg/m^3
Absorption coefficient	1.632 mm^{-1}
$F(000)$	888
Crystal size	$0.48 \times 0.45 \times 0.30$ mm^3
Theta range for data collection	1.94° to 26.00°
Limiting indices	$-10 \leq h \leq 10$, $-14 \leq k \leq 17$, $-18 \leq l \leq 19$
Reflections collected/unique	9631/3600 [R(int) = 0.0183]
Completeness to $\theta = 26.00°$	99.1%
Max. and min. transmission	0.6402 and 0.5080
Refinement method	Full-matrix least-squares on F^2
Data/restraints/parameters	3600/0/235
Goodness-of-fit on F^2	1.037
Final R indices [$I > 2\sigma(I)$][a,b]	$R_1 = 0.0289$, $wR_2 = 0.0749$
R indices (all data)	$R_1 = 0.0372$, $wR_2 = 0.0795$
Largest diff. peak and hole	0.286 and −0.182 e Å^{-3}

[a] $R_1 = \Sigma\|F_o|-|F_c\|/\Sigma|F_o|$.
[b] $wR_2 = \{\Sigma[w(F_o^2 - F_c^2)^2]/\Sigma w(F_o^2)^2]\}^{1/2}$; where $w = [\sigma^2(F_o^2) + (0.043P)^2 + 0.410P]^{-1}$ and $P = (F_o^2 + 2F_c^2)/3$.

days. The infrared spectrum of [$ZnCl_2(\eta^3$-N,N,O-dpkbh)] shows significant changes compared to the spectrum of the free ligand. The multiple bands observed in the metal complex between 3600 and 3300 cm^{-1} may be due to the participation of the amide proton in hydrogen bonding, and are in contrast to the non-hydrogen bonded amide proton in the free ligand reported at 3347 cm^{-1} [10,35]. A notable feature that significantly changed when $ZnCl_2$ binds to dpkbh is the amide ν(C=O) stretching vibration observed at 1680 cm^{-1} in the free ligand shifts to 1633 cm^{-1} in the metal complex, pointing to the coordination of the carbonyl group of dpkbh and a decrease in its bond order and an increase in C–O bond length. In the C=O stretching region ~900 cm^{-1}, the metal complex showed a significant decrease in the intensity of the peak observed at 892 cm^{-1} compared to that of the free ligand. In the combined C=C and C=N stretching vibrations of the pyridine rings, the broad peak at 1575 cm^{-1} in the free ligand splits into two sharp peaks at 1598 and 1571 cm^{-1} may be due to the binding of one nitrogen of the pyridine rings. In the amide II region ~1530 cm^{-1}, the free ligand shows two broad peaks between 1550–1490 cm^{-1} and the metal complex shows a sharp peak at 1506 cm^{-1}. The three peaks between 1300–1215 cm^{-1} which may be due to the combined C–N or N–N stretching of the free ligand merging into one sharp peak at 1262 cm^{-1} in the metal complex. This hints at the possible coordination of the hydrazone nitrogen atom. The N–H out-of-plane wagging observed at 704 cm^{-1} in the free ligand shifts to 694 cm^{-1} in the metal complex.

The NMR spectra of [$ZnCl_2(\eta^3$-N,N,O-dpkbh)] in d_7-DMF and d_6-DMSO and free dpkbh in d_6-DMSO at 30 °C are shown in Fig. 1. In the spectra of [$ZnCl_2(\eta^3$-N,N,O-dpkbh)], peaks appeared in the amide, aromatic, and solvent regions consistent with the coordination of dpkbh. The spectra of [$ZnCl_2(\eta^3$-N,N,O-dpkbh)] show sensitivity to solvent variations (see Section 2) and point to strong solvent–solute interaction. The ratio of the intensity of the amide proton to the intensity of the low field one proton of the aromatic ring is 0.5, 0.6, and 0.7 for [$ZnCl_2(\eta^3$-N,N,O-dpkbh)] in d_7-DMF and d_6-DMSO and dpkbh in d_6-DMSO. These results suggest a possible exchange of the amide proton with the protons of the incompletely deuteriated solvents with the exchange faster in d_7-DMF. The aromatic protons of [$ZnCl_2(\eta^3$-N,N,O-dpkbh)] shifting to more positive values in d_7-DMF compared to d_6-DMSO may be due to stronger hydrogen bonding interaction between d_7-DMF and the amide proton that lead to a decrease in electron density about the coordinated dpkbh [35]. A comparison of the chemical shift of the aromatic protons of [$ZnCl_2(\eta^3$-N,N,O-dpkbh)] with those of free dpkbh in d_6-DMSO shows slight changes in the splitting of resonances between 7.70–7.45 ppm and indicates that the interaction between $ZnCl_2$ and the pyridine ring is associated with these protons. The chemical shift of the amide proton is sensitive to temperature variations (see Fig. 2) consistent with solvent–solute interaction. A plot

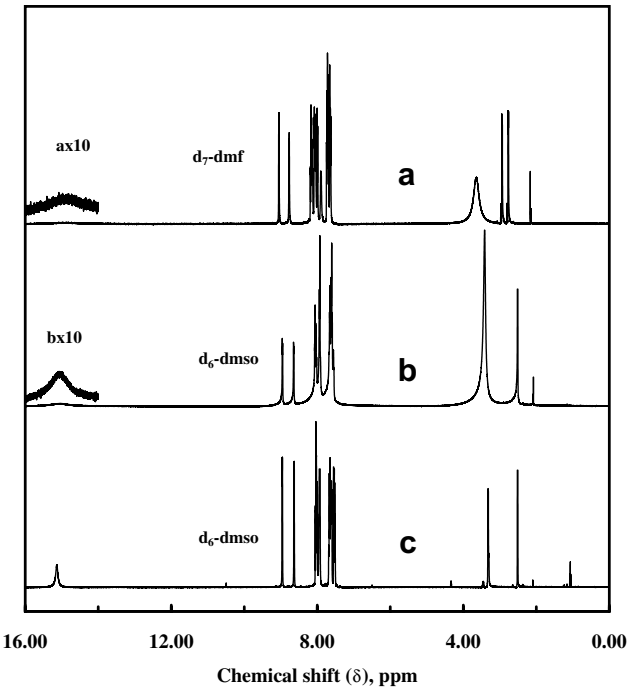

Fig. 1. ^{1}H NMR spectra of [$ZnCl_2(\eta^3$-N,N,O-dpkbh)] measured in d_6-DMSO (a), d_7-DMF (b) and dpkbh in DMSO (c) at 30 °C.

of the chemical shift of the amide versus $(1/T)/K^{-1}$ in DMF and DMSO gave straight lines with slopes of

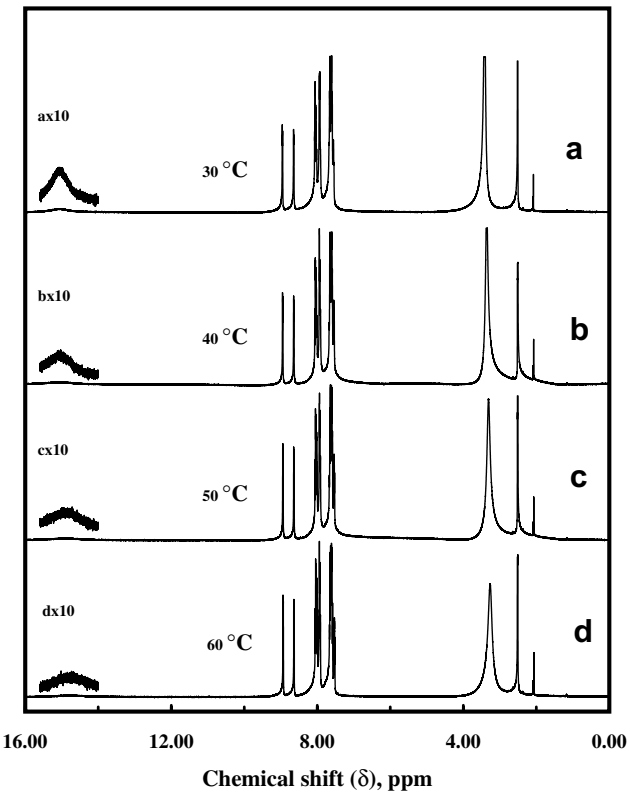

Fig. 2. ^{1}H NMR spectra of [$ZnCl_2(\eta^3$-N,N,O-dpkbh)] measured in d_6-DMSO at 30 °C (a), 40 °C (b), 50 °C (c) and 60 °C (d).

998 ± 32 and 1209 ± 54, respectively, and suggests the higher sensitivity of [$ZnCl_2(\eta^3$-N,N,O-dpkbh)] to temperature variations in d_6-DMSO compared to d_7-DMF.

The electronic absorption spectra of [$ZnCl_2(\eta^3$-N,N,O-dpkbh)] in different solvents are shown in Fig. 3 and a list of the electronic transitions is included in the experimental section. The solvent dependence of the electronic absorption confirms the strong solvent–solute interaction, as noted from NMR results. The electronic transitions are ILCT of the donor–acceptor type and may be due to π-π* transitions of the pyridine rings of dpk, followed by dpk to benzoyl charge transfer, or vice versa, and are similar to those observed of di-2-pyridyl ketone hydrazones and their metal compounds [10–12]. PM3 semi-empirical calculations on an energy minimized model, substantiated the aforementioned assignment (see Fig. 4), and gave a HOMO–LUMO energy gap of 4.98 eV.

The electronic transitions and relative abundance of two complex-substrate forms of [$ZnCl_2(\eta^3$-N,N,O-dpkbh)] are sensitive to changes in their surroundings. In a binary DMSO/DMF co-solvent system, the intensity of the low-energy electronic transition increases and the intensity of the high-energy electronic transition decreases as the volume% of DMF/DMSO increases (Fig. 5). These results confirm the sensitivity of the system to slight variations in the medium and hints at the inter-conversion between two complex-substrate forms of [$ZnCl_2(\eta^3$-N,N,O-dpkbh)]. This was confirmed when [$ZnCl_2(\eta^3$-N,N,O-dpkbh)] was subjected to chemical and physical stimuli that causes the equilibrium distribution of the species corresponding to the high- and low-energy electronic transitions

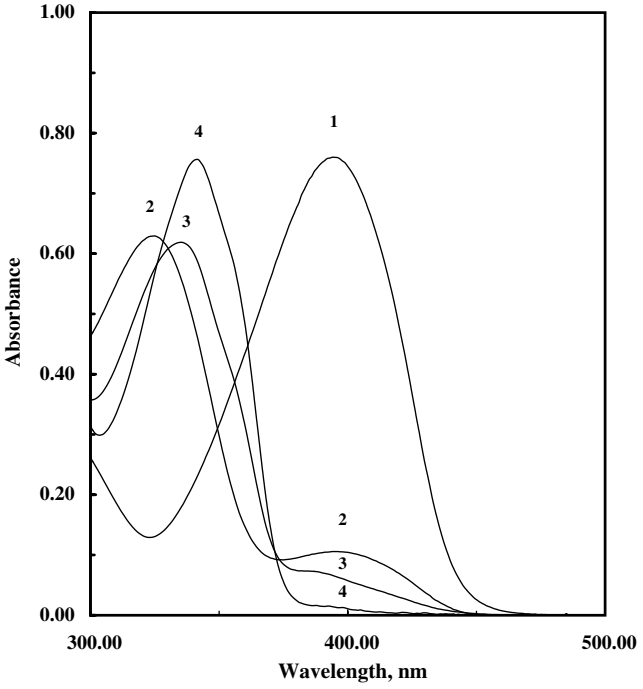

Fig. 3. The electronic absorption spectra of 4.00×10^{-5} M [$ZnCl_2(\eta^3$-N,N,O-dpkbh)] in DMF (1), DMSO (2), CH_3CN (3) and CH_2Cl_2 (4).

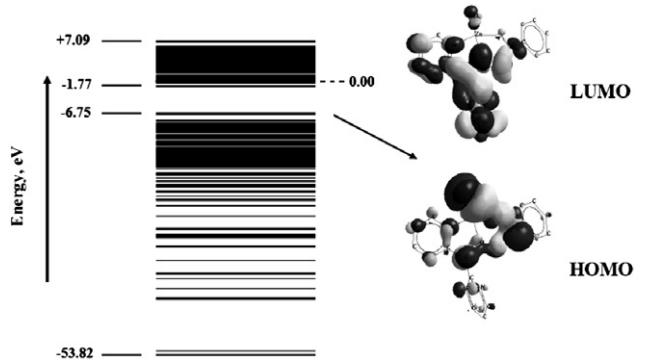

Fig. 4. Semi-empirical energy level diagram of a Hyperchem AMBER energy minimized [$ZnCl_2(\eta^3$-N,N,O-dpkbh)].

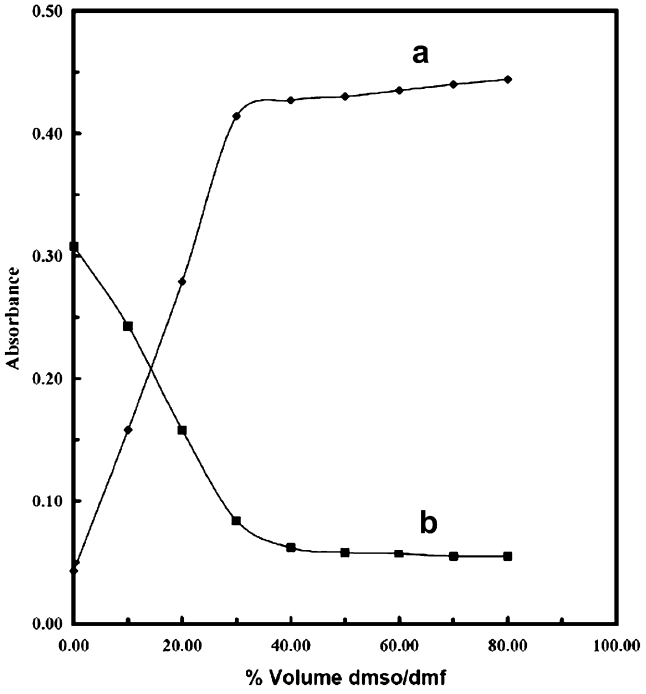

Fig. 5. A plot of the absorbance of [$ZnCl_2(\eta^3$-N,N,O-dpkbh)] versus volume% of DMSO/DMF co-solvent at 396 nm (a) and 324 nm (b).

(henceforth denoted as β and α, respectively). Fig. 6 shows the spectra of a mixture of [$ZnCl_2(\eta^3$-N,N,O-dpkbh)] and $NaBH_4$ in DMSO when allowed to react with increasing amounts of KPF_6. Under these conditions the electronic spectra of the resulting solutions show the intensity of the low-energy electronic transition to decrease and the intensity of the high-energy electronic transition to increase upon an increase in the concentration of KPF_6. The same was observed when increasing amounts of $NaBF_4$ were added to a DMF solution of [$ZnCl_2(\eta^3$-N,N,O-dpkbh)]. The reverse was obtained when a DMSO solution of [$ZnCl_2(\eta^3$-N,N,O-dpkbh)] was allowed to react with increasing amounts of $NaBH_4$. These results support reversible inter-conversion between the two states of [$ZnCl_2(\eta^3$-N,N,O-dpkbh)] and allowed for calculation of the extinction coefficients ε of the α and β forms at

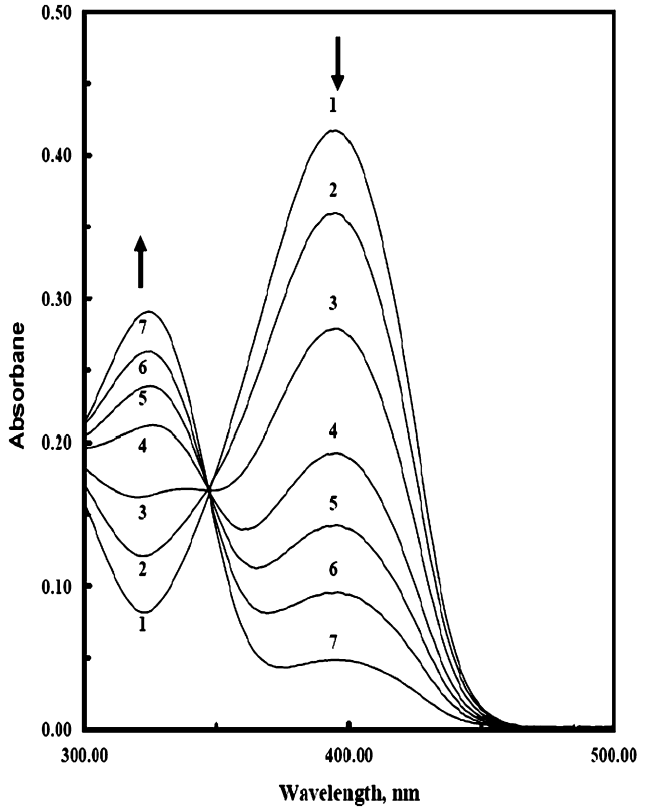

Fig. 6. Electronic absorption spectra of a mixture of [$ZnCl_2$(η^3-N,N,O-dpkbh)] 4.00×10^{-5} M and 4×10^{-5} M $NaBH_4$ in DMSO in the presence of (1) 5.00×10^{-4}, (2) 3.00×10^{-3}, (3) 8.00×10^{-3}, (4) 2.00×10^{-2}, (5) 4.00×10^{-2}, (6) 6.00×10^{-2} and (7) 8.00×10^{-2} M KPF_6.

arbitrary wavelengths. Values for ε at the two wavelengths of interest are given in Table 2.

Our results show that the optical behavior of [$ZnCl_2$(η^3-N,N,O-dpkbh)] in DMF in the presence and absence of $NaBH_4$ and in DMSO in the presence of $NaBH_4$ is similar but different from that observed in pure DMSO. The exact nature of the interaction between [$ZnCl_2$(η^3-N,N,O-dpkbh)] and different solvents or solutions remains to be elucidated.

The electronic absorption spectra of [$ZnCl_2$(η^3-N,N,O-dpkbh)] in polar solvents showed a marked variation with temperature. In DMF, when temperature is increased, the intensity of the low-energy transition peak (α) decreases, while that of the high-energy transition (β) increases. The opposite was observed when temperature was decreased or when DMSO was used in place of DMF. Plots of $R\ln K$ vs $(10^3/T)/K^{-1}$ [1] yielded straight lines with slopes of +23.3 and −14.1 and intercepts of −51 and +31 in DMF and DMSO, respectively.

Table 2
Extinction coefficients of [$ZnCl_2$(η^3-N,N,O-dpkbh)] in DMF and DMSO (±100, in $M^{-1}\,cm^{-1}$)

Solvent	$\varepsilon^{\alpha}_{320}$	$\varepsilon^{\beta}_{320}$	$\varepsilon^{\alpha}_{400}$	$\varepsilon^{\beta}_{400}$
DMF	3125	15,500	20,700	1000
DMSO	3665	15,700	20,900	0

These results substantiate that the equilibrium between the configurational states allows for calculation of the thermodynamic parameters (see Table 3) pertaining to interconversion between the configurations of [$ZnCl_2$(η^3-N,N,O-dpkbh)] in DMF and DMSO. The absorbance measurements demonstrate the facile conversion between states and their high sensitivity to slight changes in the composition of the surrounding medium and possible use as molecular probes for sensing purposes.

When [$ZnCl_2$(η^3-N,N,O-dpkbh)] in DMSO (total concentration $c=4\times10^{-5}$ M) was allowed to interact with added $ZnCl_2$, the intensity of the peak at 400 nm corresponding to the electronic transition of the α form was found to increase, while at the same time the intensity of the peak at 320 nm (corresponding to electronic absorption in the β form) decreased (Fig. 7). A plot of the absorbance versus concentration of $ZnCl_2$ is shown in Fig. 8 and shows that $ZnCl_2$ in concentrations as low as 1×10^{-5} M can be detected and determined using [$ZnCl_2$(η^3-N,N,O-dpkbh)] in DMSO. The extent of binding of $ZnCl_2$ with [$ZnCl_2$(η^3-N,N,O-dpkbh)] can be estimated from the following model

$$\beta\text{-}[ZnCl_2(\eta^3\text{-N, N, O-dpkbh})] \leftrightarrow \alpha\text{-}[ZnCl_2(\eta^3\text{-N, N, O-dpkbh})] \quad (1)$$

$$\alpha\text{-}[ZnCl_2(\eta^3\text{-N, N, O-dpkbh})] + ZnCl_2 \leftrightarrow \alpha'\text{-}[ZnCl_2(\eta^3\text{-N, N, O-dpkbh})]\cdot ZnCl_2 \quad (2)$$

where β is the form observed at the high-energy transition, α that observed at the low-energy transition and α′ is the form associated with the binding of $ZnCl_2$ to [$ZnCl_2$(η^3-N,N,O-dpkbh)].

The total absorbance at any wavelength λ, $A_\lambda=\varepsilon^{\alpha}_{\lambda}[\alpha]+\varepsilon^{\beta}_{\lambda}[\beta]$, can be expressed in terms of the equilibrium constant $K=[\alpha]/[\beta]$ for the inter-conversion of α and β and total concentration $c=[\alpha]+[\beta]$ as

[1] For the following inter-conversion:

$\beta[ZnCl_2(\eta^3\text{-N, N, O-dpkbh})] \rightleftarrows \alpha[ZnCl_2(\eta^3\text{-N, N, O-dpkbh})]$

the total absorbance at wavelength λ equals $A_\lambda=\varepsilon^{\alpha}_{\lambda}[\alpha]+\varepsilon^{\beta}_{\lambda}[\beta]=\varepsilon^{\beta}_{\lambda}c+(\varepsilon^{\alpha}_{\lambda}-\varepsilon^{\beta}_{\lambda})[\alpha]$, where $c=[\alpha]+[\beta]$ is the total concentration. Thus, $[\alpha]=(A_\lambda-\varepsilon^{\beta}_{\lambda}c)/(\varepsilon^{\alpha}_{\lambda}-\varepsilon^{\beta}_{\lambda})$, so that the equilibrium constant $K=[\alpha]/[\beta]$ at temperature T equals

$$K(T)=\frac{A_\lambda(T)-\varepsilon^{\beta}_{\lambda}c}{\varepsilon^{\alpha}_{\lambda}c-A_\lambda(T)},$$

which should be independent of λ (the occurrence of an isosbestic point in the spectra at different temperatures indicates that the extinction coefficients are temperature independent). The data thus obtained should then be substituted into the thermodynamic relationship

$$-\frac{\Delta G^{\theta}}{T}=R\ln K=\Delta S^{\theta}-\frac{\Delta H^{\theta}}{T},$$

where $\Delta X=X_\alpha-X_\beta$, so that a plot of $R\ln K$ vs. $1/T$ should yield a straight line with slope $-\Delta H^{\theta}$ and intercept ΔS^{θ}.

Table 3
Thermodynamic parameters for the inter-conversion between the two forms of [Zn(η^3-N,N,O-dpkbh)Cl_2]

Solvent	ΔH^0/kJ mol^{-1}	ΔS^0/J mol^{-1}K^{-1}	ΔG^0/kJ mol^{-1} (25 °C)	K (25 °C)
DMF	-23.3 ± 0.5	-51 ± 4	-8.16 ± 0.02	27.0 ± 0.2
DMSO	$+14.1 \pm 0.2$	$+31 \pm 2$	$+4.54 \pm 0.61$	0.16 ± 0.04

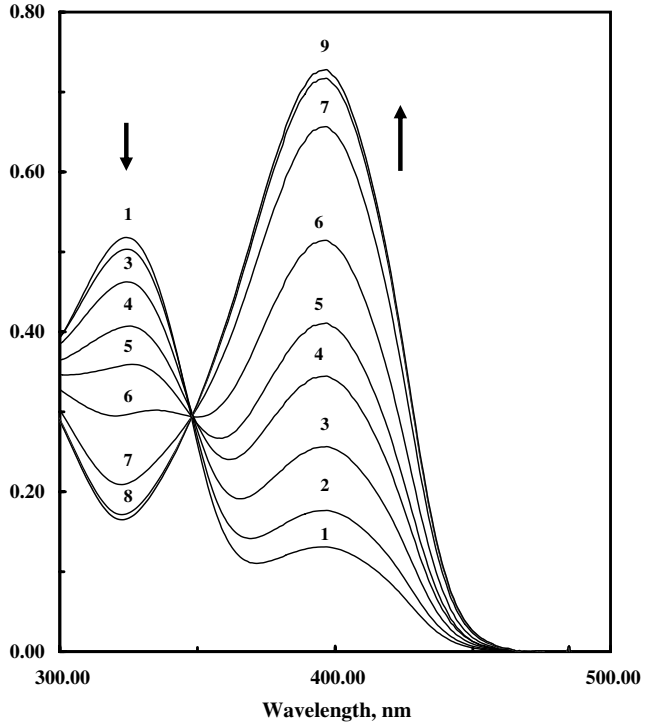

Fig. 7. Electronic absorption spectra of [$ZnCl_2$(η^3-N,N,O-dpkbh)] 4.00×10^{-5} M in DMSO in the presence of (1) 0.00, (2) 1.00×10^{-4}, (3) 3.00×10^{-4}, (4) 5.00×10^{-4}, (5) 1.00×10^{-3}, (6) 3.00×10^{-3}, (7) 5.00×10^{-3}, (8) 7.00×10^{-3} and (9) 9×10^{-3} M $ZnCl_2$.

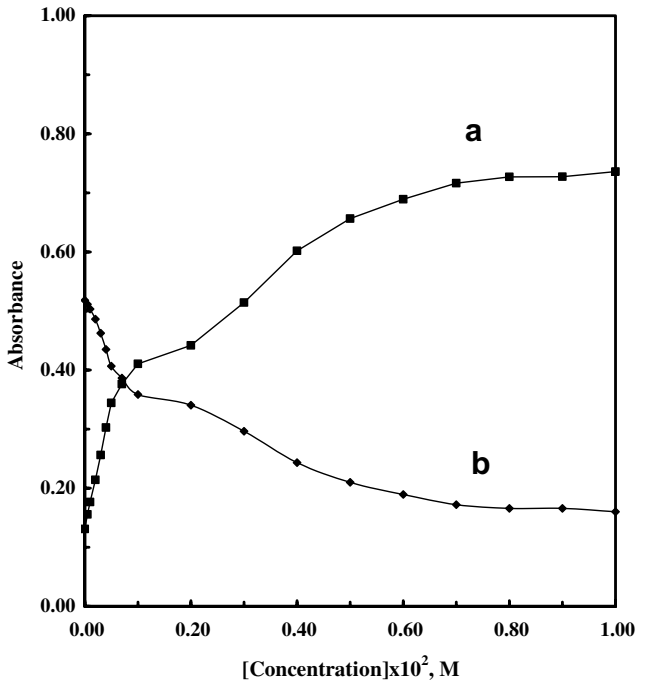

Fig. 8. A plot of the absorbance of [$ZnCl_2$(η^3-N,N,O-dpkbh)] 4.00×10^{-5} M in DMSO at 396 and 324 nm, respectively, versus concentration of $ZnCl_2$.

$$A_\lambda = \frac{K\varepsilon_\lambda^\alpha + \varepsilon_\lambda^\beta}{1+K} c, \tag{3}$$

so that, once the extinction coefficients ε for α and β at λ (which, to simplify the notation, are taken to include the path length $l = 1$ cm) are known, this can be used to find K (which should, of course, be independent of λ) from the slope σ_λ of a plot of A_λ vs c, as obtained from a simple dilution experiment, according to

$$K = \frac{\varepsilon_\lambda^\beta - \sigma_\lambda}{\sigma_\lambda - \varepsilon_\lambda^\alpha}. \tag{4}$$

Application of this model gave K values of 27.0 and 0.16 in DMF and DMSO, respectively.

When $ZnCl_2$ is added to a solution of [$ZnCl_2$(η^3-N,N,O-dpkbh)] the following relations are obeyed at equilibrium

$$[\alpha] + [\alpha'] + [\beta] = [\alpha'] + (1 + K^{-1})[\alpha] = c, \tag{5}$$

and

$$[\mathrm{M}] = [\mathrm{M}]_\mathrm{T} - [\alpha'] = [\mathrm{M}]_\mathrm{T} + (1 + K^{-1})[\alpha] - c, \tag{6}$$

where [M] = concentration of free $ZnCl_2$ and $[\mathrm{M}]_\mathrm{T}$ = total concentration of $ZnCl_2$, and the binding constant for (2) is defined as

$$K' = \frac{[\alpha']}{[\mathrm{M}][\alpha]}. \tag{7}$$

Substitution of (6) and (7) into (5) leads to the following quadratic equation in terms of [α],

$$K'(1 + K^{-1})[\alpha]^2 + (1 + K^{-1} + K'([\mathrm{M}]_\mathrm{T} - c))[\alpha] - c = 0, \tag{8}$$

The absorbance at some wavelength λ is equal to

$$\begin{aligned} A_\lambda &= \varepsilon_\lambda^\alpha([\alpha] + [\alpha']) + \varepsilon_\lambda^\beta[\beta] \\ &= \varepsilon_\lambda^\alpha c + (\varepsilon_\lambda^\beta - \varepsilon_\lambda^\alpha)[\alpha]/K. \end{aligned} \tag{9}$$

After inserting the solution of (8) into (9), solving the resulting equation for K' and using (4) we obtain, after some lengthy algebra,

$$K' = \frac{(\varepsilon_\lambda^\beta - \varepsilon_\lambda^\alpha)(\sigma_\lambda - \varepsilon_\lambda^\alpha)(A_\lambda - \sigma_\lambda c)}{(\sigma_\lambda - \varepsilon_\lambda^\beta)(A_\lambda - \varepsilon_\lambda^\alpha c)(A_\lambda - \sigma_\lambda c + [\mathrm{M}]_\mathrm{T}(\sigma_\lambda - \varepsilon_\lambda^\alpha))}, \tag{10}$$

which should produce the same value of K', regardless of the chosen spectrum (i.e. $ZnCl_2$ concentration) and value of λ (except the one corresponding to the isosbestic point where the extinction coefficients of α and β are equal). The values for the extinction coefficients at the wavelengths of interest in this study, 320 and 400 nm, have been obtained using the spectral shifts towards either α or β form in different solvents via addition of $NaBH_4$ and/or KPF_6. To check the reliability of these values, and the internal consistency of the model, a general relationship between extinction coefficients at different wavelengths can be derived based on the following argument.

From (9) and the mass balance equation (3) it follows that $A_\lambda - \varepsilon_\lambda^\alpha c = (\varepsilon_\lambda^\beta - \varepsilon_\lambda^\alpha)[\beta]$ and similarly $A_\lambda - \varepsilon_\lambda^\beta c = (\varepsilon_\lambda^\alpha - \varepsilon_\lambda^\beta)([\alpha] + [\alpha'])$, which are valid for each spectrum in Fig. 7. If we compare any two spectra, henceforth denoted by superscripts (1) and (2), the first of these relations implies that

$$\frac{A_{320}^{(1)} - \varepsilon_{320}^\alpha c}{A_{400}^{(1)} - \varepsilon_{400}^\alpha c} = \frac{A_{320}^{(2)} - \varepsilon_{320}^\alpha c}{A_{400}^{(2)} - \varepsilon_{400}^\alpha c} = \frac{\varepsilon_{320}^\beta - \varepsilon_{320}^\alpha}{\varepsilon_{400}^\beta - \varepsilon_{400}^\alpha}, \tag{11}$$

which is clearly independent of the choice of the two spectra, and so therefore is the first equality, which can be reorganized to

$$(A_{400}^{(1)} - A_{400}^{(2)})\varepsilon_{320}^\alpha + (A_{320}^{(2)} - A_{320}^{(1)})\varepsilon_{400}^\alpha = (A_{320}^{(2)}A_{400}^{(1)} - A_{320}^{(1)}A_{400}^{(2)})/c. \tag{12}$$

The second form of (9) leads to an identical linear equation for ε_{320}^β and ε_{400}^β. Based on the data of Fig. 7, this relationship takes the form $\varepsilon_{320}^{\alpha,\beta} + 0.58\varepsilon_{400}^{\alpha,\beta} = 15,700$ for the solutions in DMSO. The analogous relationship for the solutions in DMF is somewhat similar, $\varepsilon_{320}^{\alpha,\beta} + 0.63\varepsilon_{400}^{\alpha,\beta} = 16,130$. The values for ε listed in Table 2 are seen to be reasonably consistent with these equations. This same linear relationship can be readily shown to exist also between the slopes σ_{320} and σ_{400} of the dilution plots, as a consequence of the fact that in (3), K should be independent of λ. Moreover, in view of the requirement that K' as obtained from (10) should be invariant with respect to changes in λ, it is possible to show that this relationship also applies to A_{320}/c and A_{400}/c for arbitrary $[M]_T$. Compliance with these conditions can be verified from direct inspection of the dilution plots and spectra. Our data for the solutions in DMSO imply $K = 0.16$ and support a value of K' somewhere in the range 6000–8000 M^{-1}. The latter follows after repeated application of (10) to the spectra of Fig. 7 at the two chosen wavelengths and different concentrations of added $ZnCl_2$. A similar calculation for the case of DMF was not feasible because the α form is already strongly favored by the solvent itself.

The electrochemical properties of [$ZnCl_2$(η^3-N,N,O-dpkbh] were investigated using voltammetric techniques. Cyclic voltammograms of [$ZnCl_2$(η^3-N,N,O-dpkbh] measured in DMF are shown in Fig. 9. In a reductively initiated scan (Fig. 9a), two closely-spaced irreversible

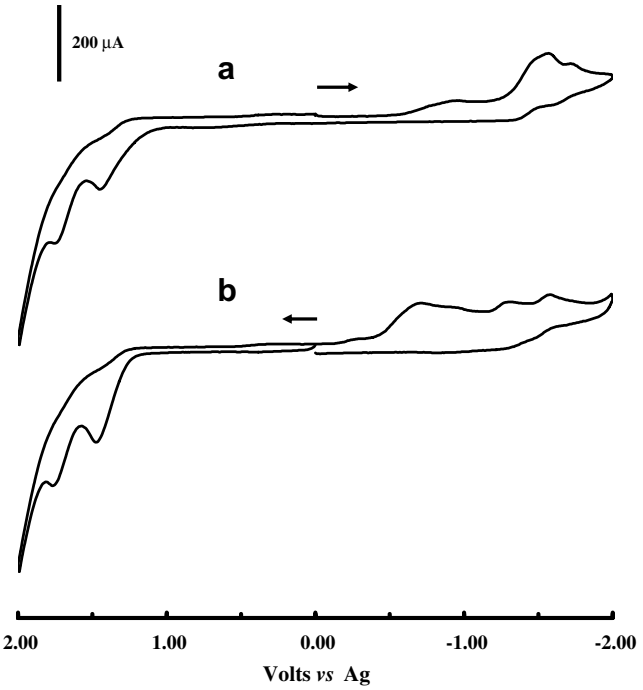

Fig. 9. Cyclic voltammograms of [$ZnCl_2$(η^3-N,N,O-dpkbh] in DMF solutions (0.1 M in [N(*n*-Bu)$_4$]PF_6 at a glassy carbon working electrode recorded at a scan rate of 400 mV s^{-1}.

reductions appeared at $E_{p,c} = -0.78$ and -0.93 V and closely-spaced multi-electron irreversible reductions appeared at $E_{p,c} = -1.47$, -1.58, and -1.75 V, followed by multi-

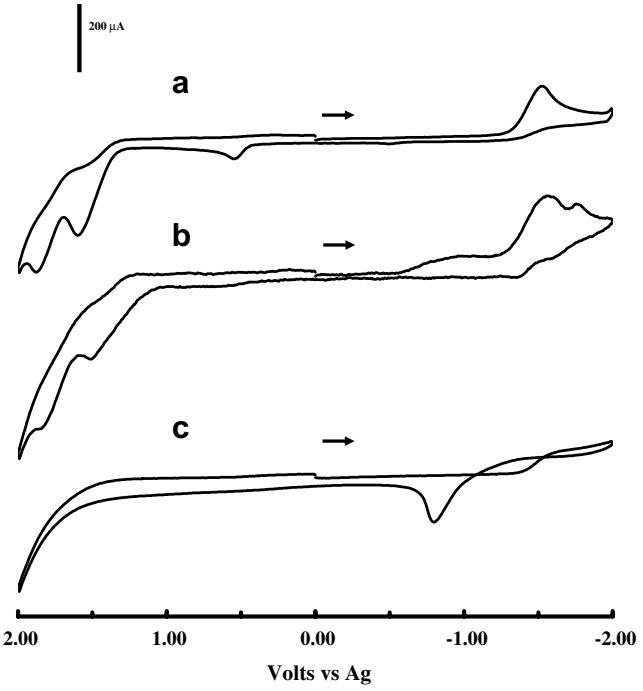

Fig. 10. Cyclic voltammograms of dpkbh measured in the absence (a) and in the presence of $ZnCl_2$ (b) along with a cyclic voltammogram of $ZnCl_2$ (c) measured in DMF solutions 0.1 M in [N(*n*-Bu)$_4$]PF_6 at a glassy carbon working electrode measured at a scan rate of 400 mV s^{-1}.

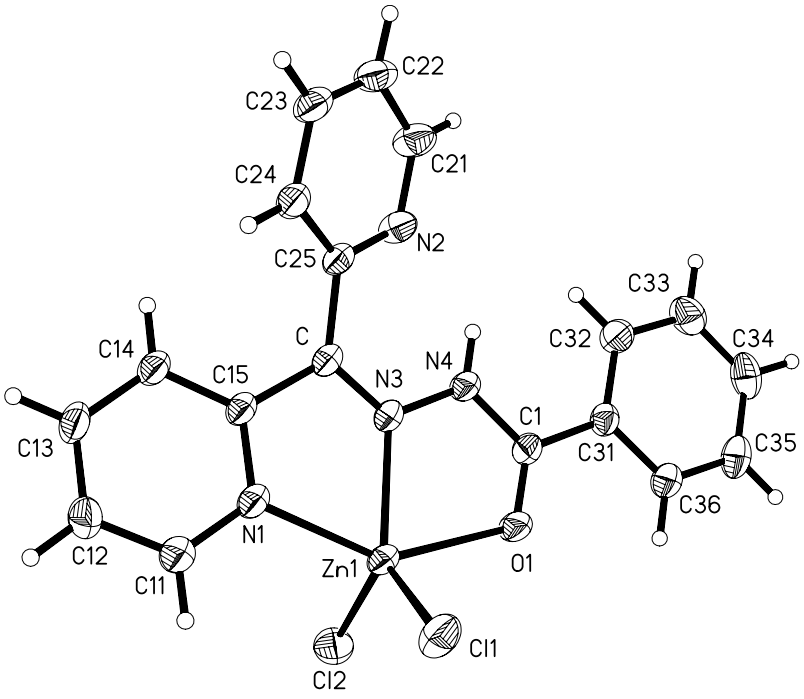

Fig. 11. The molecular structure of [$ZnCl_2$(η^3-N,N,O-dpkbh)]. The thermal ellipsoids are drawn at the 30% probability level and H atoms are shown as small spheres of arbitrary radii.

electron irreversible oxidations at $E_{p,a} = +1.42$ and +1.76 V. A reductive square wave voltammogram measured on the same solution confirmed the redox potentials observed in a reductively initiated cyclic voltammogram. The first two closely-spaced reductions can be assigned to $Zn^{2+/+}$ and $Zn^{+/0}$ reductions and the other waves may be due to ligand-based reductions. In an oxidatively-initiated scan (see Fig. 9b), irreversible oxidations appeared at $E_{p,a} = +1.46$ and 1.74 V, followed by an electrochemically-generated product wave at $E_{p,c} = -0.67$ (broad) and irreversible reductions at $E_{p,c} = -0.91$, -1.26 and -1.55 V. The appearance of an oxidatively generated product wave upon oxidatively-initiated scan signals oxidative decomposition of [$ZnCl_2$(η^3-N,N,O-dpkbh]. The oxidative decomposition of [$ZnCl_2$(η^3-N,N,O-dpkbh] remains to be explored.

The electrochemical reaction of dpkbh with $ZnCl_2$ was investigated. Fig. 10 shows reductively-initiated cyclic voltammograms measured in DMF of dpkbh in the presence and absence of $ZnCl_2$, along with the voltammogram of pure $ZnCl_2$. These voltammograms show the addition of $ZnCl_2$ to a DMF solution of dpkbh leading to an electrochemical signature similar to that of [$ZnCl_2$(η^3-N,N,O-dpkbh] measured in DMF, and hints at a facile reaction between dpkbh and $ZnCl_2$. The absence of electrochemically-generated product waves upon coordination of $ZnCl_2$ to dpkbh, as apparent from the absence of the reductively generated oxidative waves observed at $E_{p,a} = +0.45$ V in free dpkbh (Fig. 10a), suggests increased stability of dpkbh upon coordination to $ZnCl_2$. The appearance of $Zn^{2+/0}$ reduction waves at more positive values compared to the free $ZnCl_2$ suggests a decrease in the electron density of $ZnCl_2$ upon coordination to dpkbh.

The solid state structure of [$ZnCl_2$(η^3-N,N,O-dpkbh)] was determined using X-ray structural analysis. A view of the molecular structure of [$ZnCl_2$(η^3-N,N,O-dpkbh)] is shown in Fig. 11 and reveals pseudo trigonal-bipyramidal coordination about zinc with an index of trigonality (τ) = 0.33 indicating that the irregular coordination geometry of [$ZnCl_2$(η^3-N,N,O-dpkbh)] in the solid state is 33% along the pathway of distortion from square-pyramidal to trigonal-bipyramidal [36].[2] The coordinated atoms are two chlorine atoms and one nitrogen atom of the hydrazone moiety of dpkbh occupy the equatorial positions and the axial positions are occupied by a nitrogen atom of the coordinated pyridine ring and the oxygen atom of the benzoyl moiety. The coordinated dpkbh forms two five-membered metallocyclic rings (Zn1–N1–C15–C–N3) and (Zn1–N3–N4–C–O1) fused along the Zn–N junction and leaves one pyridine ring exposed for potential binding to other substrates. The N–N and N–O bite angles of 73.05(6)° and 71.85(6)°, respectively are significantly smaller than the 90° between the axial and equatorial ligands. The phenyl ring and hydrazone backbone are co-planar, and non-coplanar with the pyridyine rings. Deviation from trigonal bipyramidal geometry is due to the tridentate binding of η^3-N,N,O-dpkbh as apparent from the N–N

[2] For a five-coordinate system similar to that shown in Fig. 11, the trigonality index $\tau = (\beta - \alpha)/60$ where $\beta = \angle$N1–Zn1–O1, $\alpha = \angle$N3–Zn1–Cl1. Thus $\tau = 0$ for a perfect tetragonal geometry and $\tau = 1$ for a perfect trigonal-bipyramidal geometry.

Table 4
Bond lengths [Å] and angles [°] for $ZnCl_2(\eta^3$-N,N,O-dpkbh)

Bond lengths			
Zn(1)–N(1)	2.1679(16)	Zn(1)–N(3)	2.1452(16)
Zn(1)–Cl(2)	2.2232(8)	Zn(1)–Cl(1)	2.2267(8)
Zn(1)–O(1)	2.2274(14)	N(1)–C(11)	1.331(3)
N(1)–C(15)	1.348(3)	C(11)–C(12)	1.379(3)
C(12)–C(13)	1.363(3)	C(15)–C	1.494(3)
C–N(3)	1.297(2)	C–C(25)	1.483(3)
N(2)–C(21)	1.326(3)	N(2)–C(25)	1.347(3)
C(21)–C(22)	1.383(3)	C(22)–C(23)	1.366(3)
N(3)–N(4)	1.354(2)	N(4)–C(1)	1.366(2)
C(1)–O(1)	1.225(2)	C(1)–C(31)	1.473(3)
C(31)–C(32)	1.382(3)	C(31)–C(36)	1.393(3)
C(32)–C(33)	1.376(3)		
Bond angles			
N(3)–Zn(1)–N(1)	73.05(6)	N(1)–Zn(1)–Cl(2)	101.39(5)
N(3)–Zn(1)–Cl(1)	124.89(5)	Cl(2)–Zn(1)–Cl(1)	116.07(3)
N(3)–Zn(1)–O(1)	71.85(6)	N(1)–Zn(1)–O(1)	144.76(6)
Cl(1)–Zn(1)–O(1)	96.68(5)	C(11)–N(1)–C(15)	118.53(17)
C(11)–N(1)–Zn(1)	122.85(13)	C(15)–N(1)–Zn(1)	117.22(13)
N(1)–C(15)–C(14)	121.53(18)	N(1)–C(15)–C	114.02(16)
C(14)–C(15)–C	124.33(17)	N(3)–C–C(25)	124.67(18)
N(3)–C–C(15)	112.44(16)	C(25)–C–C(15)	122.84(16)
C(21)–N(2)–C(25)	117.97(18)	N(2)–C(21)–C(22)	123.7(2)
N(2)–C(25)–C	115.77(16)	C(24)–C(25)–C	122.23(18)
C–N(3)–N(4)	121.79(16)	C–N(3)–Zn(1)	120.58(13)
N(4)–N(3)–Zn(1)	116.28(11)	N(3)–N(4)–C(1)	115.79(15)
O(1)–C(1)–N(4)	119.66(17)	O(1)–C(1)–C(31)	123.17(17)
N(4)–C(1)–C(31)	117.17(17)	C(1)–O(1)–Zn(1)	116.36(12)
C(32)–C(31)–C(36)	118.93(19)	C(32)–C(31)–C(1)	123.43(18)
C(36)–C(31)–C(1)	117.63(18)	C(33)–C(32)–C(31)	120.4(2)

and N–O bite angles of coordinated atoms (see Table 4). The tridentate binding mode of dpkbh is in contrast to the bidentate N,N-binding mode of dpkbh observed in *fac*-$[Re(CO)_3(\eta^2$-N,N-dpkbh)X], *fac*-$[Re(CO)_3(\eta^2$-N,N-dpkbh)Cl]·solvate, where X = Cl or Br and solvate = DMSO or DMF and dpkbh binds to the metal cen-

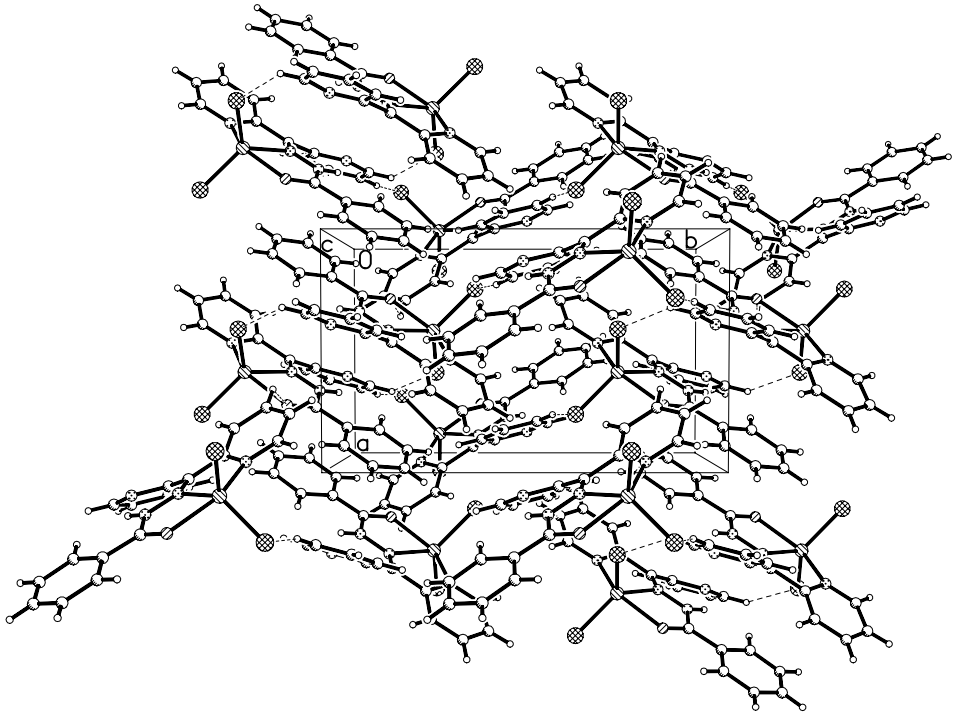

Fig. 12. A view of the packing of $[ZnCl_2(\eta^3$-N,N,O-dpkbh)].

ter through the nitrogen atoms of the pyridine rings, and *fac*-[Re(CO)$_3$(η^2-N,N-dpkbh)Br]·thf where dpkbh binds to the metal center through a nitrogen atom of a pyridine ring and the nitrogen atom of the hydrazone backbone and is similar to the binding mode of dpkbh in [$ZnCl_2$(Brdpkbh)], [Fe(dpkbh)$_2$] and other related compounds of N,N,O-tridentate di-2-pyridyl ketone hydrazones [11,12,30,32,37].

The packing of molecules shows digitated stacks of [$ZnCl_2$(η^3-N,N,O-dpkbh)] connected via a network of hydrogen bonds (see Fig. 12 and Table 5). The chlorine and oxygen atoms of [$ZnCl_2$(η^3-N,N,O-dpkbh)] participate in non-classical intermolecular hydrogen bonds of the type C–H···X where X = Cl or O (see Fig. 13). The amide proton is in close proximity to the nitrogen atom of the uncoordinated pyridine ring and participates in a classical intramolecular hydrogen bond of the type N–H···N (see Fig. 13). The covalent and non-covalent bond distances and angles are normal and similar to those observed in dpkbh and a variety of its compounds [10–12].

Table 5
Hydrogen bonds for $ZnCl_2$(η^3-N,N,O-dpkbh) [Å and °]

D–H···A	*d*(D–H)	*d*(H···A)	*d*(D···A)	<(DHA)
N(4)–H(4)···N(2)	0.86	1.98	2.605(2)	128.9
C(13)–H(13)···O(1)^1	0.93	2.57	3.167(3)	122.4
C(21)–H(21)···Cl(2)^2	0.93	2.78	3.504(3)	135.1
C(22)–H(22)···Cl(1)^3	0.93	2.82	3.668(2)	151.5

Symmetry transformations used to generate equivalent atoms: $^1x-1/2$, $-y+3/2$, $z-1/2$; ^2-x, $-y+1$, $-z+2$ and $^3-x+1/2$, $y-1/2$, $-z+3/2$.

4. Summary

Spectroscopic measurements on solutions of [$ZnCl_2$(η^3-N,N,O-dpkbh)] isolated from the reaction between $ZnCl_2$ and dpkbh in acetonitrile under reflux or ultrasonic radiation show sensitivity of [$ZnCl_2$(η^3-N,N,O-dpkbh)] to slight changes in its surroundings. Thermodynamic and optosensing studies reveal that facile inter-conversion between two ILCT transitions and substrates in concentrations as low as 1×10^{-5} M can be detected and determined using [$ZnCl_2$(η^3-N,N,O-dpkbh)] in polar solvents. X-ray structural studies on [$ZnCl_2$(η^3-N,N,O-dpkbh)] confirmed its identity and revealed digitated stacks of [$ZnCl_2$(η^3-N,N,O-dpkbh)] interconnected via a network of hydrogen bonds. In view of the convenient synthesis of di-2-pyridyl ketone hydrazones and their metal compounds, their interesting physico-chemical properties and potential use in the development of molecular sensors, studies are underway in our laboratory to further explore the coordination

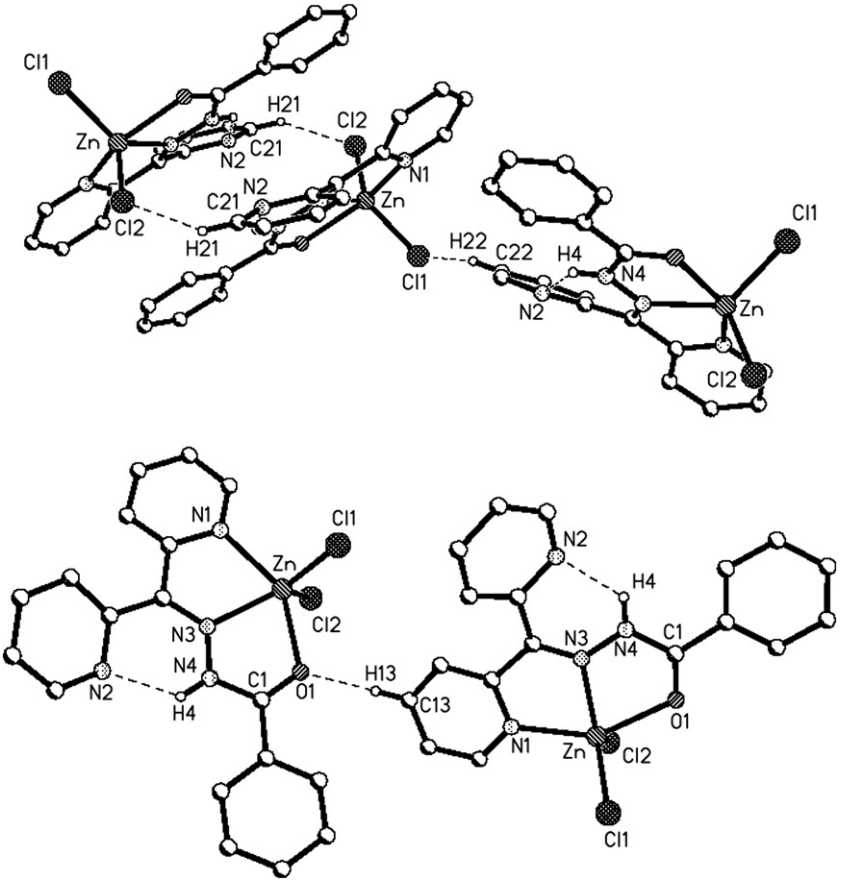

Fig. 13. Views of the hydrogen bonds in [$ZnCl_2$(η^3-N,N,O-dpkbh)].

chemistry and sensing behavior of this and other di-2-pyridyl ketone derivatives.

Acknowledgments

We acknowledge Ms. Toni Johnson for her assistance with the NMR measurements and Dr. Bohari M. Yamin for performing the X-ray measurements.

References

[1] Y.-C. Liu, C.-I. Li, W.-Y. Yeh, G.-H. Lee, S.-M. Peng, Inorg. Chim. Acta 359 (2006) 2361.
[2] M.C. Tseng, J.L. Ke, C.C. Pai, S.P. Wang, W.L. Huang, Polyhedron 25 (2006) 2160.
[3] V. Philip, V. Suni, M.R.P. Kurup, M. Nethaji, Polyhedron 25 (2006) 1931.
[4] C.J. Milios, S. Piligkos, A.R. Bell, R.H. Laye, S.J. Teat, R. Vicente, E. McInnes, A. Escuer, S.P. Perlepes, R.E.P. Winpenny, Inorg. Chem. Commun. 9 (2006) 638.
[5] S. Youngme, J. Phatchimkun, U. Suksangpanya, C. Pakawatchai, G.A. van Albada, M. Quesada, J. Reedijk, Inorg. Chem. Commun. 9 (2006) 242.
[6] P.V. Bernhardt, J. Mattsson, D.R. Richardson, Inorg. Chem. 23 (2006) 752.
[7] X.-D. Chen, T.C.W. Mak, Inorg. Chim. Acta 359 (2006) 685.
[8] M. Bakir, O. Green, C. Gyles, Inorg. Chim. Acta 358 (2005) 1835.
[9] M. Bakir, C. Gyles, J. Mol. Struct. 753 (2005) 35.
[10] M. Bakir, O. Brown, J. Mol. Struct. 609 (2002) 129.
[11] M. Bakir, O. Brown, Inorg. Chim. Acta 353 (2003) 89.
[12] M. Bakir, O. Brown, T. Johnson, J. Mol. Struct. 691 (2004) 265.
[13] M. Bakir, K. Abdur-Rashid, C. Gyles, Spectrochim. Acta Part A 59 (2003) 2123.
[14] M. Bakir, C. Gyles, J. Mol. Struct. 649 (2003) 133.
[15] M. Bakir, K. Abdur-Rashid, Trans. Metal Chem. 24 (1999) 384.
[16] M. Bakir, K. Abdur-Rashid, W.H. Mulder, Talanta 51 (2000) 735.
[17] M. Bakir, C. Gyles, Talanta 56 (2002) 1117.
[18] M. Bakir, O. Brown, J. Mol. Struct. 641 (2002) 183.
[19] M. Bakir, Eur. J. Inorg. Chem. (2002) 481.
[20] M. Bakir, Inorg. Chim. Acta 332 (2002) 1.
[21] M. Bakir, O. Green, Acta Cryst. C58 (2002) 263.
[22] M. Bakir, Acta Cryst. C57 (2001) 1371.
[23] M. Bakir, Acta Cryst. C57 (2001) 1154.
[24] M. Bakir, J.A.M. McKenzie, J. Electroanal. Chem. 425 (1997) 61.
[25] M. Bakir, J.A.M. McKenzie, J. Chem. Soc. Dalton Trans. (1997) 3571.
[26] M. Bakir, J. Electroanal. Chem. 466 (1999) 60.
[27] M. Bakir, I. Hassan, O. Green, J. Mol. Struct. 657 (2003) 75.
[28] J.J. Pinto, C. Moreno, M. García-Vargas, Talanta 64 (2004) 562.
[29] L.H.S.A. Terra, M. Guekezian, I. Gaubeur, J.R. Matos, M.E.V. Suárez-Iha, Polyhedron 21 (2002) 2375.
[30] J. Grewea, A. Hagenbacha, B. Stromburga, R. Albertob, E. Vazquez-Lopez, U. Abrama, Z. Anorg. Allg. Chem. 629 (2003) 303.
[31] P.V. Bernhardt, J. Mattsson, D.R. Richardson, Inorg. Chem. 45 (2006) 752.
[32] P.V. Bernhardt, L.M. Caldwell, T.B. Chaston, P. Chin, D.R. Richardson, J. Biol. Inorg. Chem. 8 (2003) 866.
[33] Bruker-SHELXTL, Software Version 5.1. Brucker AXS, Inc., Madison, Wisconsin, USA, 1997.
[34] G.M. Sheldrick, SHELX97 and SHELXL97, University of Göttingen, Germany, 1997.
[35] R.M. Silverstein, F.X. Webster, Spectroscopic Identification of organic Compounds, sixth ed., John Wiley and Sons Inc., New York, 1997.
[36] A.W. Addison, T.N. Rao, J. Reedijk, J.v. Rijn, G.C. Verschoor, J. Chem. Soc, Dalton Trans. (1984) 1349.
[37] C.E. Kyriakidis, P.C. Christidis, P.J. Rentzeperis, I.A. Tossidis, Z. Kristallogr. 193 (1990) 261.